# Ta2C precipitation after low pressure carburizing of tantalum

Dominique Cotton, Philippe Jacquet, Sébastien Faure, Vincent Vignal

# $Ta_2C$ precipitation after low pressure carburizing of tantalum

Dominique Cotton [a,*], Philippe Jacquet [a,b], Sébastien Faure [c], Vincent Vignal [d]

[a] Arts et Métiers Institute of Technology, LaBoMaP, HESAM Université, 71250, Cluny, France
[b] Ecole Catholique des Arts et Métiers, LabECAM, 40 montée saint Barthélémy, 69005, Lyon, France
[c] CEA, DAM, Valduc, 21100, Is-sur-Tille, France
[d] ICB, UMR 6303 CNRS, Université de Bourgogne-Franche Comté, BP 47870, 21078, Dijon Cedex, France

- This paper presents the first research work about $Ta_2C$ precipitates layer growth.
- Tantalum matrix vacancies are consumed during the precipitation of $Ta_2C$.
- $Ta_2C$ precipitation is reduced close to vacancy sinks (grain boundary, surface, …).
- $Ta_2C$ precipitation is also reduced in zones where $Ta_2C$ precipitates had appeared at least once.
- An annealing treatment following a carburizing treatment increase the $Ta_2C$ precipitates layer growth.

*Keywords:*
Tantalum
Carburizing
$Ta_2C$
Annealing

A B S T R A C T

Low pressure carburizing cycles were carried out on tantalum samples. A $Ta_2C$ precipitates layer is present under the TaC and $Ta_2C$ surface layers. As the TaC and $Ta_2C$ layers, the $Ta_2C$ precipitates layer (TPL) grows by carbon diffusion in tantalum matrix. Specific zones with low precipitates content were observed at the bulk surface and in the tantalum grain boundaries. Other zones with lower precipitates content are also present in carburized and annealed samples. All the zones with low precipitates content are induced by the $Ta_2C$ precipitation mechanism described by Dahmen et al. [1,2]. Indeed, $Ta_2C$ needs vacancies to precipitate. If vacancy sinks are present at the bulk surface, at a grain boundary or in a dislocation, then $Ta_2C$ precipitation is highly reduced. Another effect of the annealing treatment is an increase of the $Ta_2C$ precipitates layers growth rate.

## 1. Introduction

Tantalum carbides were highly studied in the 60's for their interesting properties (high melting point, high hardness …). TaC and $Ta_2C$ carbides can be obtained on tantalum parts by carburizing [1]. First, $Ta_2C$ layer appears at the tantalum surface. Then the supersaturation in carbon of $Ta_2C$ causes a TaC layer at the surface [2]. These carbide layers were obtained by many carburizing processes [3–6]. The diffusion of carbon is the main mechanism that leads to these carbides growth as shown in the literature [3,6,7].

The Ta/C phase diagram, given by Gusev et al. [8] (Fig. 1), shows the range of existence of the two main carbides TaC and $Ta_2C$. These carbides could exist in a non-stoechiometric form. TaC can contain between 42.5 and 50% at.% carbon. $Ta_2C$ has two allotropic phases, α-Ta2C (ordered carbon sublattice, $CdI_2$ antitype structure) and β-$Ta_2C$ (disordered carbon sublattice, L'3 structure). An allotropic transformation between α and β-$Ta_2C$ occurs at approximately 1677 °C [8–10]. This transformation has been observed by thermal analysis by Rudy et al. [11]. This compound exists for a small concentration range, between 26 and 33.3% at. of carbon and his melting point is 3330 °C [11]. Two other carbides are described in the phase diagram: $Ta_4C_3$ and $Ta_6C_5$. $Ta_4C_3$ was described for the first time by Lesser et al. [7]. It is a rhombohedral carbide (R3m space group) that appears in the presence of TaC and $Ta_2C$ [12]. $Ta_6C_5$ is an ordered phase created by the order/disorder transition of non-stoichiometric TaC [8]. These two carbides appear after long annealing times.

After a carburizing cycle on tantalum, a strong decrease of the carbon solubility limit causes a carbon saturation during its cooling [12–16],

* Corresponding author. Arts et Métiers, Rue Porte de Paris, 71250, Cluny, France.
*E-mail addresses:* dominique.cotton@ensam.eu (D. Cotton), philippe.jacquet@ecam.fr (P. Jacquet), sebastien.faure@cea.fr (S. Faure), vincent.vignal@u-bourgogne.fr (V. Vignal).

https://doi.org/10.1016/j.matchemphys.2021.125632

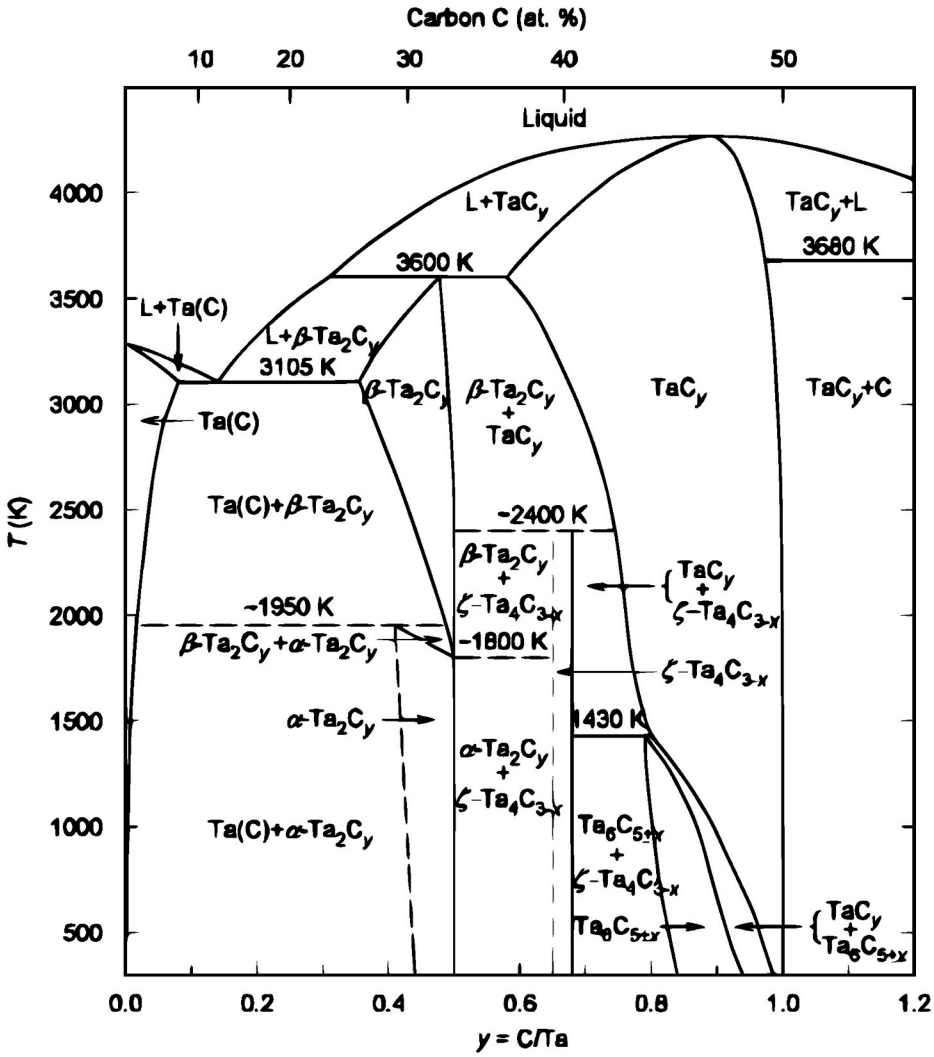


**Fig. 1.** Ta/C phase diagram [8].

**Table 1**
Concentration of impurities determined by GDMS.

| Element | Na | Mg | Al | Si | S | K | Ti |
|---|---|---|---|---|---|---|---|
| Wt ppm | <0.01 | <0.001 | 0.25 | 0.52 | <0.005 | <0.01 | 0.003 |
| Element | Cr | Mn | Fe | Pb | Co | Ni | Cu |
| Wt ppm | 0.09 | <0.005 | 1.4 | <0.005 | <0.001 | <0.001 | 0.14 |
| Element | Zn | Zr | Nb | Mo | C | Ta | W |
| Wt ppm | <0.005 | 0.11 | 36 | 0.81 | <0.05 | Matrix | 0.25 |

from 7.5 %at C at 2843 °C [11] to 0.08 %at C at room temperature [13, 16]. Then $Ta_2C$ precipitates appear scattered in the tantalum supersaturated matrix. $Ta_2C$ precipitation was also observed by Rudy et al. [11] with a highly exothermic reaction as evidenced by a DTA-thermogram. Dahmen et al. [17,18] highlight the contribution of vacancies on $Ta_2C$ precipitation. The present study shows that these precipitates could appear as layers under TaC and $Ta_2C$ ones. These carbides layers growth were highly studied in many different processes, and will not be studied in this paper. In the literature dealing with $Ta_2C$ precipitates [11,14, 18–24], they are always described as filling the tantalum matrix, and never as layers under tantalum carbides layers. However, as far as we know, there are no previous studies about $Ta_2C$ precipitates layers growth. The aim of this paper is the characterization of these $Ta_2C$ precipitates and especially of their distribution. Moreover, the influence of parameters such as carburizing and annealing time has been approached.

**Table 2**
Concentration of impurities determined by IGA.

| Element | C | N | O | S | H |
|---|---|---|---|---|---|
| wt ppm | <5 | 20 | 10 | - | 4,7 |

## 2. Experimental

High purity (99.99%) tantalum samples (10 mm in diameter and 2 mm thick, from a rolled round bar) were used in this study. The chemical composition has been verified by GDMS Table 1) and IGA (Table 2).

The initial microstructure is composed of various grain sizes, form 1–40 μm, and determined by EBSD, with a TSL EDAX OIM XM detector. $Ta_2C$ precipitates appear during the carburizing treatment of tantalum. The carburizing has been made at low pressure, with a BMicro furnace.

**Table 3**
Experimental plan.

| Carburizing temperature (°C) | 1400 | | | 1600 | | | | | | | | | | | |
|---|---|---|---|---|---|---|---|---|---|---|---|---|---|---|---|
| Carburizing time (min) | 60 | 120 | 240 | 60 | | | | 120 | | | | 240 | | | |
| Annealing time (min) | | 0 | | 0 | 30 | 60 | 120 | 0 | 30 | 60 | 120 | 0 | 30 | 60 | 120 |

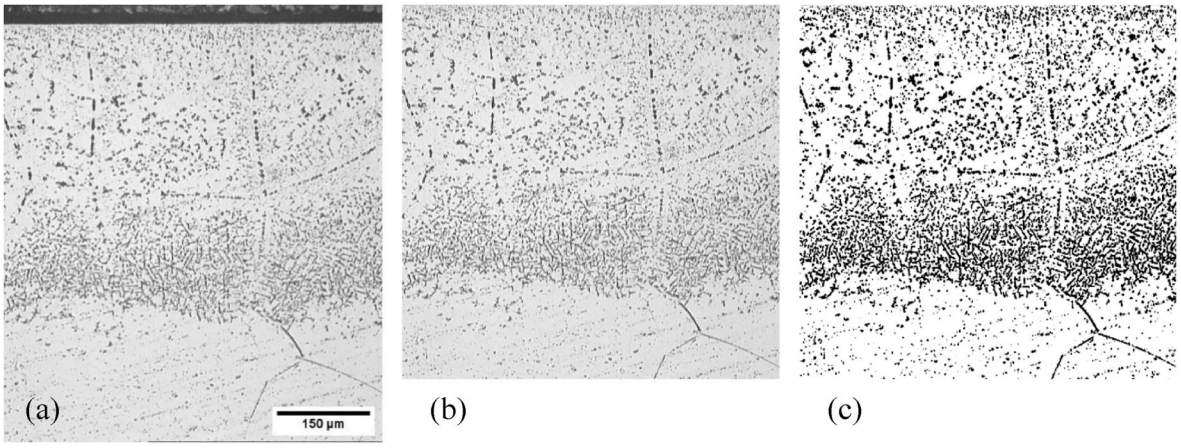


**Fig. 2.** Optical cross section image of a tantalum sample carburized for 20 min and annealed for 60 min, (a): Original image, (b): Cropped image, (c): Binarized image.

The carburizing treatment involves several steps: primary vacuum in the chamber, heating, carburizing and cooling. The carburizing temperature was reached with a rate of 30 °C/min. The carburizing gas was ethylene ($C_2H_4$, 99.99% of purity) at a pressure of 20 mbar, with a gas flow rate of 20 L/h. The heating resistors of the furnace and the sample holder was made in graphite. Gas pressure has been measured with a Baratron capacitance gauge for pressures in the range of few mbar, and with a Pirani gauge for pressures in the range of $10^{-2}$ mbar. Two temperatures were investigated (1400 °C and 1600 °C) and three carburizing times (60, 120 and 240 min). The highest temperature tested here is 1600 °C (1873K), so the $Ta_2C$ carbide formed by precipitation should only be α-$Ta_2C$ (Fig. 1). The temperature in the furnace chamber was controlled by two Type C molybdenum sheathed thermocouples, placed between the resistors and the samples. After the carburizing cycle, samples were cooled under 1 bar of nitrogen. Some carburized samples were then annealed, for 30 min–120 min at 1600 °C. The experimental plan is described in Table 3, each experiment has been carried once, with one tantalum sample in the chamber:

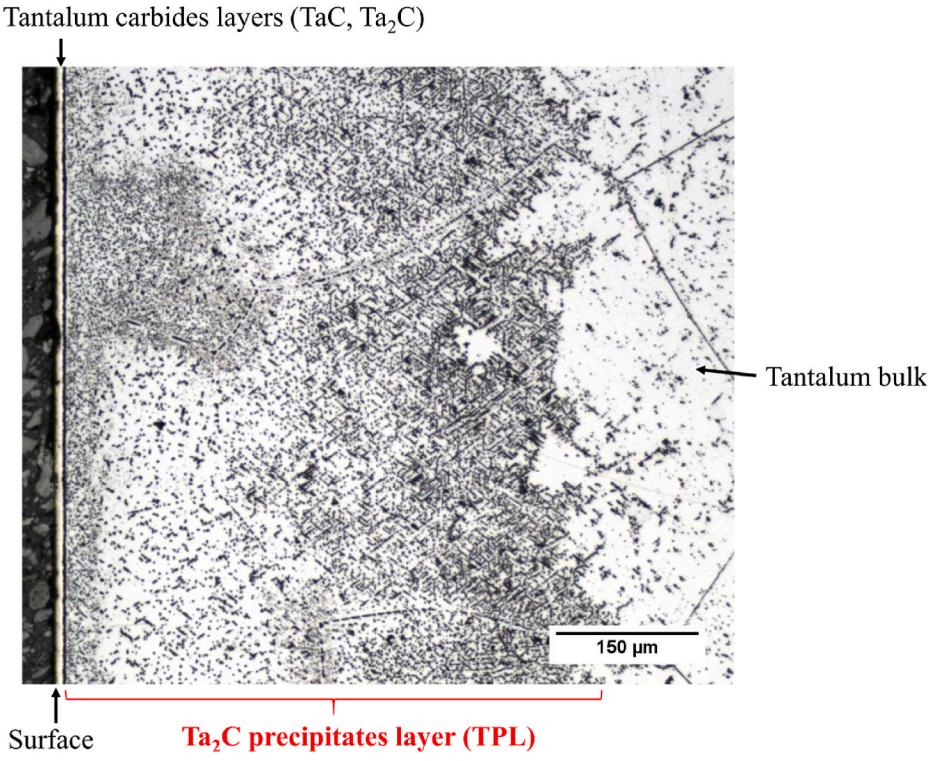


**Fig. 3.** Optical cross section of a carburized sample: 240 min at 1600 °C (etching HF + $HNO_3$).

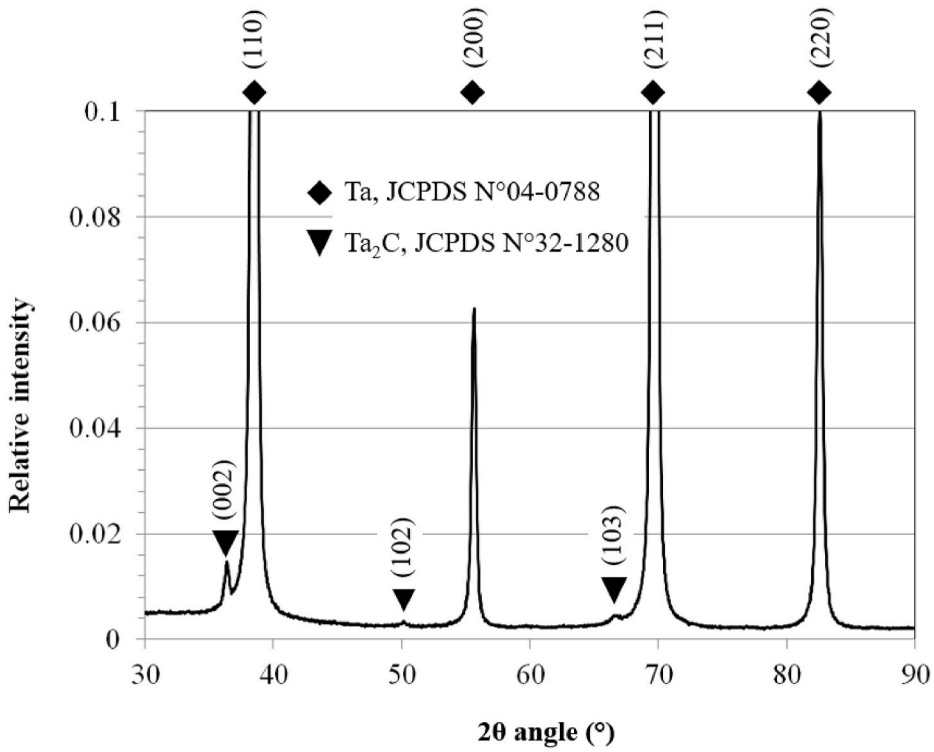


**Fig. 4.** XRD patterns of a sample carburized 60 min at 1600 °C.

Annealed samples were cooled under primary vacuum (~$10^{-2}$ mbar). After treatments, the samples were cut and cross sections were polished with SiC papers then colloidal silica solution. $Ta_2C$ precipitates were revealed by etching, with a combination of strong acids (13% vol. HF + 23% vol. $HNO_3$ + 64% vol. $H_2O$). This etching recipe is derived from the publication of Chang et al. [25].

The $Ta_2C$ precipitates density has been determined from optical images with ImageJ software as shown in Fig. 2. First, images were cropped in order to remove surface carbide layers or artifacts such as the scale bar. Next, images were binarized with a threshold of 191/255. Black pixels depict $Ta_2C$ precipitates, etching pits and grain boundaries. We assumed that the values found below the $Ta_2C$ precipitates layer are due to etching pits and etched grain boundaries.

Then, the density of pixels was calculated for each row of pixels, from the surface to the bulk material. For each row, the total amount of black pixels is divided by the total number of pixels. Each row of pixel is 0.8 µm thick. Then we obtained a graph representing the $Ta_2C$ precipitates density as a function of the depth observed. Curves were smoothed with

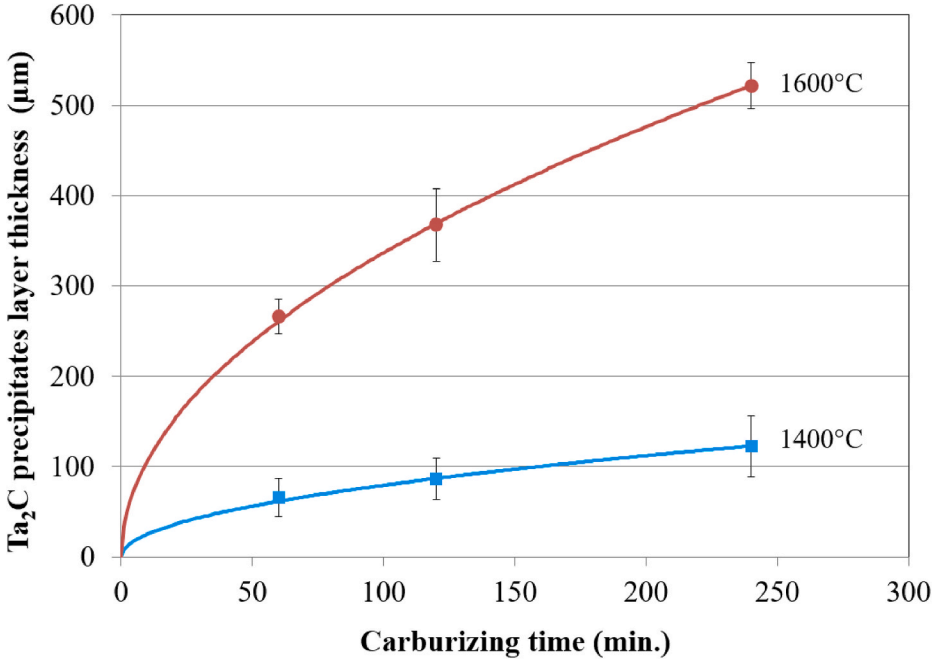


**Fig. 5.** $Ta_2C$ precipitates layer thickness vs. carburizing time.

**Table 4**
Growth constants of TPL.

| Carburizing temperatures (°C) | Growth constants ($\mu m^2/s$) |
|---|---|
| 1400 | 1.04 |
| 1600 | 18.92 |

a floating mean calculated with 30 values.

The average thickness of the $Ta_2C$ precipitate layers were measured from three optical images where 20 measurements were carried out. $Ta_2C$ precipitates pictures have been made with an Eclipse L150 microscope. For the need of the publication of this article, other micrographs have been made later with a BM51X microscope (Figs. 3, 7 and 9).

The microstructure of the treated samples was identified by XRD (XRG 3000 Inel diffractometer) using a copper radiation source ($\lambda_{Co}$ = 0.1541 nm) at 40 kV and 40 mA at the source (Bragg-Brentano configuration). The XRD patterns have been compared with JCPDS databases to identify compounds. An acquisition time of 15 h has been necessary to reduce the signal/noise ratio, in order to get $Ta_2C$ peaks on the XRD patterns.

Vickers hardness indentations were made using a BUELHER 1600–6300 microhardness tester with a 100 g load.

## 3. Results and discussion

### 3.1. Carburizing of tantalum samples

Fig. 3 shows an optical cross section image of the $Ta_2C$ precipitates layer (TPL) which appears under carbides layers. The region between tantalum bulk and the precipitates is irregular but well defined.

In order to identify the nature of the precipitates, XRD analysis was carried out on a carburized sample (60 min at 1600 °C). The surface of the sample was previously polished to remove carbide layers. Three Vickers indentations measured before and after polishing the sample were used to determine the thickness of the removed metal that was 505 ± 50 µm.

Only two compounds were identified on the XRD patterns (Fig. 4): one can note the diffraction peaks characteristic of the tantalum substrate and only three diffraction peaks characteristic of $Ta_2C$. The theoretical main diffraction peak of $Ta_2C$ (101) located at 44.5° can't be detected as it is superimposed with the Ta (100) one. Therefore, it is not possible to calculate the exact amount of $Ta_2C$. Nevertheless, as the $Ta_2C$ peaks intensities are very low compared to the Ta ones, we expect a low amount of $Ta_2C$ in the Ta matrix.

The $Ta_2C$ precipitates layers thickness as a function of the carburizing time is reported in Fig. 5.

These measurements were fitted by a parabolic law for each carburizing temperature. This law can be expressed by the usual equation (1) [3–6]:

$$W = \sqrt{kt} \tag{1}$$

where $W$ is the precipitates layer thickness (µm), $k$ is a growth constant (temperature dependent, $\mu m^2/s$) and $t$ is the carburizing time (s).

The obtained curves confirm that the TPL growth is driven by carbon diffusion in tantalum as reported by Kidson [26]. The growth constants, $k$, were determined from equation (1) and Fig. 4 and are reported in Table 4.

These growth constants are higher than TaC and $Ta_2C$ growth constants. For example, Rocher [2] showed growth constants of $7.56 \times 10^{-4}$ $\mu m^2/s$ and $3.28 \times 10^{-3}$ $\mu m^2/s$ for TaC layer growth, respectively at 1400 °C and 1600 °C. This is probably due to a higher carbon diffusion coefficient, 4 order of magnitude higher in tantalum than in TaC or $Ta_2C$ [3,6,13].

$Ta_2C$ precipitates optical images also showed (Fig. 3) an irregular region between the TPL and tantalum matrix, which induced non accurate TPL thickness measurements. These thickness variations are located inside and at grain boundaries, and could be explained by an increased carbon diffusion coefficient. It has been observed in the case of other diffusion couples such as carbon/niobium [27]. Then we could expect that some crystalline defects, like grain boundaries or subgrain boundaries could influence carbon diffusion coefficient in tantalum.

The density of $Ta_2C$ precipitates were measured on carburized tantalum samples (Fig. 6). The three measurements were carried out at different locations of the surface sample and permitted to verify the reproducibility of the measurements. The density is not homogeneous in the bulk of the sample: it varies from 65% near the surface from 27% at 200 µm of depth (zone A). Then, the density reaches 65% at 450 µm of depth (zone B) and finally decreases (zone C) and remains constant (15%) in the bulk of the sample (zone D). The 15% constant level depicts the density of etching pits due to the chemical etching on tantalum.

The density of precipitates is driven by the mechanism reported by Dahmen et al. [17,18] and Westmacott [28]. $Ta_2C$ precipitates need vacancies to appear during the cooling stage after the carburizing.

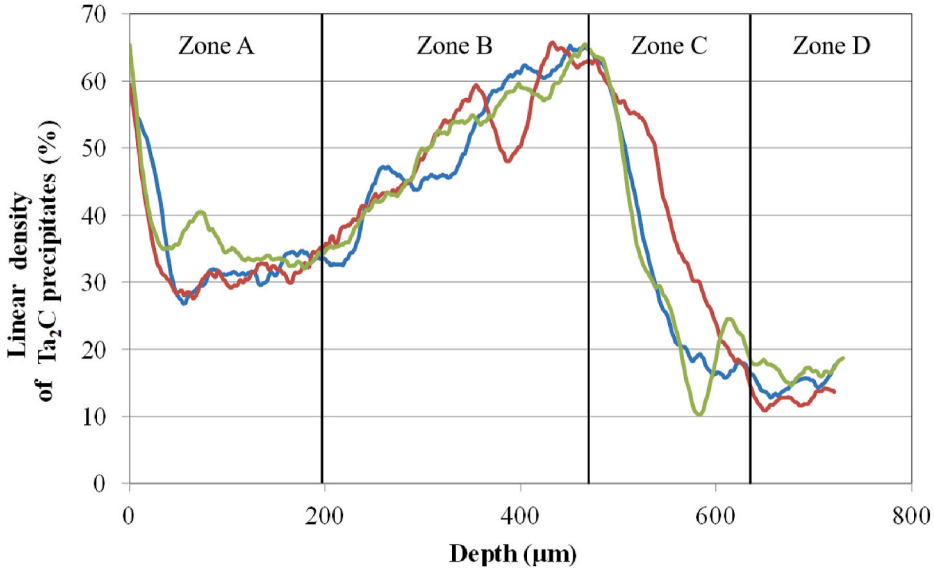


**Fig. 6.** Linear density of $Ta_2C$ precipitates for a carburized sample during 240 min at 1600 °C.

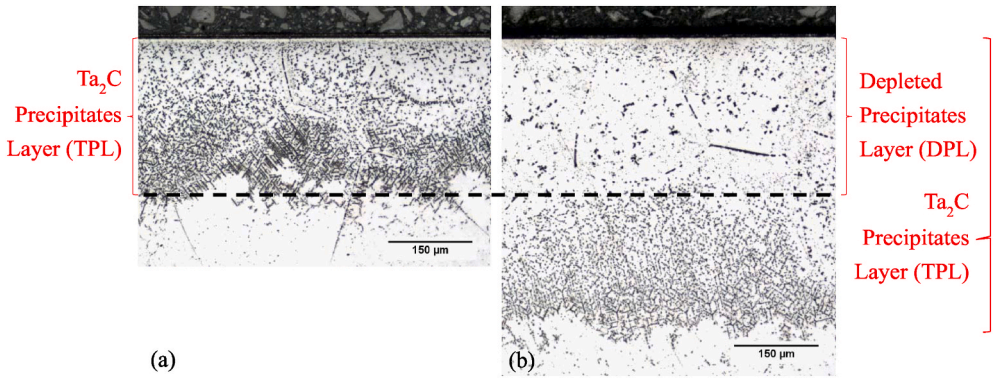


**Fig. 7.** Optical cross section images: of a carburized sample during 1h at 1600 °C)(a) and of a carburized (1h/1600 °C) and annealed (1h/1600°c) sample (b).

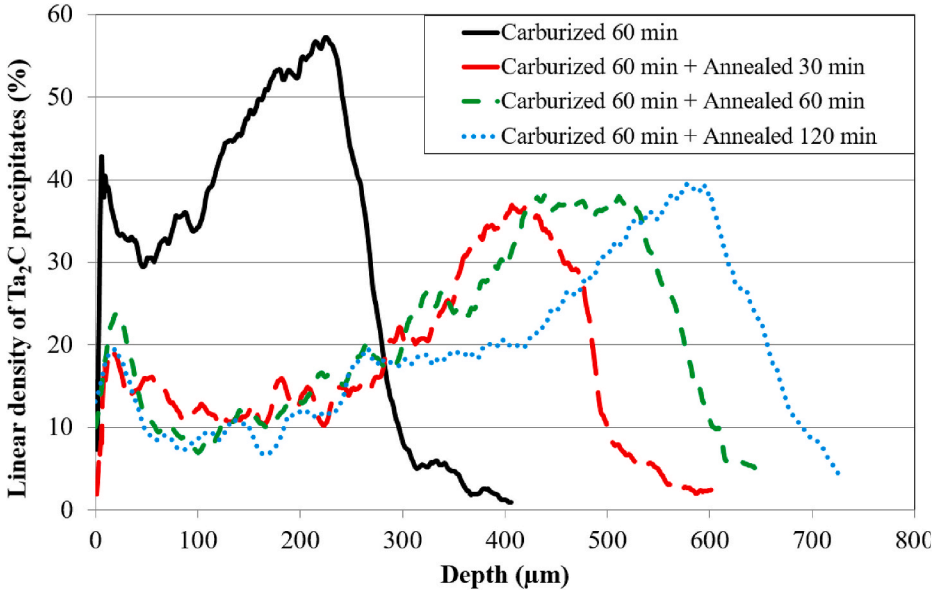


**Fig. 8.** Linear density of $Ta_2C$ precipitates for a carburized and carburized + annealed sample.

During this cooling stage, carbon solubility in tantalum decreases, resulting in carbon atoms still in solid solution. When the carbon concentration reaches its limit of solubility in Ta, the carbon atoms diffuse towards the surrounding vacancies. Vacancy-carbon atom complexes align themselves on {310} tantalum planes, to form $Ta_2C$ coherent platelets. During their growth the $Ta_2C$ precipitates become progressively incoherent but keep their crystalline orientations. Indeed, during the precipitates formation, vacancies disappear by local collapse of the tantalum lattice. bulk surface, dislocations and grain boundaries are vacancy sinks [28]. Therefore $Ta_2C$ precipitation is reduced near these lattice defaults. The low value of precipitates density in the zone A could be probably due to the diffusion of vacancies to the bulk surface. Concerning the high value of precipitates density in the first 50 µm of depth, it remains yet unexplained.

### 3.2. *Annealing of the carburized tantalum samples*

#### 3.2.1. *$Ta_2C$ precipitates distribution in the TPL*

The annealing treatment changes the $Ta_2C$ precipitates distribution in the TPL (Fig. 6).

As shown in Fig. 7a) and b), the $Ta_2C$ precipitates thickness increases from 266 µm to 543 µm after annealing at 1600 °C during 60 min. A new region with a low amount of precipitates appears after annealing (region DPL, for Depleted Precipitates Layer). It is obvious that the thickness of the TPL before annealing corresponds exactly to the thickness of this new region.

The thicker TPL after annealing is probably due to carbon diffusion. Indeed, during the annealing treatment, the increasing of the limit of solubility of carbon in Ta produced the dissolution of the $Ta_2C$ precipitates. The carbon in solid solution has then diffused in the bulk of the sample. The TaC and $Ta_2C$ carbide layers at the surface also supplied carbon to the tantalum substrate by diffusion.

The $Ta_2C$ precipitates in the bulk surface of the annealed sample are probably due to the co-precipitation of $Ta_2C$ [18]. Indeed, after the first carburizing treatment, the $Ta_2C$ precipitates are produced at the cooling stage from the supersaturated solution of carbon in tantalum. Then, vacancies initially existing in tantalum are consumed during the precipitation of $Ta_2C$. The annealing treatment is then carried out, allowing the carbon to diffuse deeper into tantalum. During the cooling stage of the annealing treatment, $Ta_2C$ precipitates appear in the remaining vacancies under the previous TPL. In the DPL region, the vacancies did not reappear during the annealing treatment preventing $Ta_2C$ precipitation.

Measurements of precipitates density were carried out on carburized and annealed samples (Fig. 8) for different annealing times. The annealing time has no effect on the precipitates density near the surface sample where the amount of $Ta_2C$ precipitates is relatively low (~10% in region DPL). One can note that it corresponds to the higher $Ta_2C$ precipitates content in the case of the only carburized sample. This result

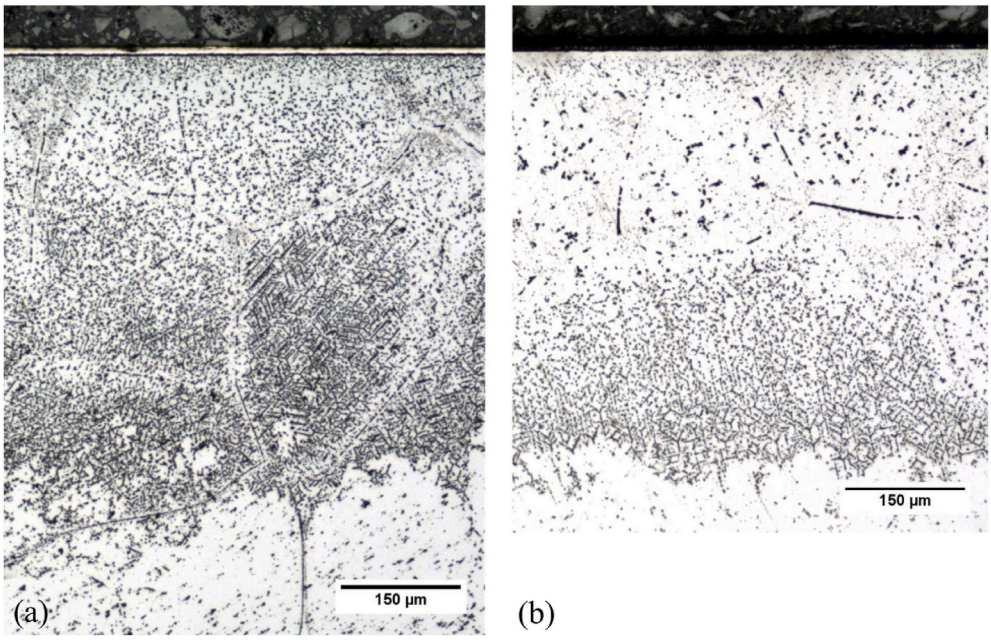


**Fig. 9.** Optical cross section images of $Ta_2C$ precipitates layers in, (a) a carburized sample 240 min/1600 °C, (b) a carburized 60 min + annealed 60 min/1600 °C sample.

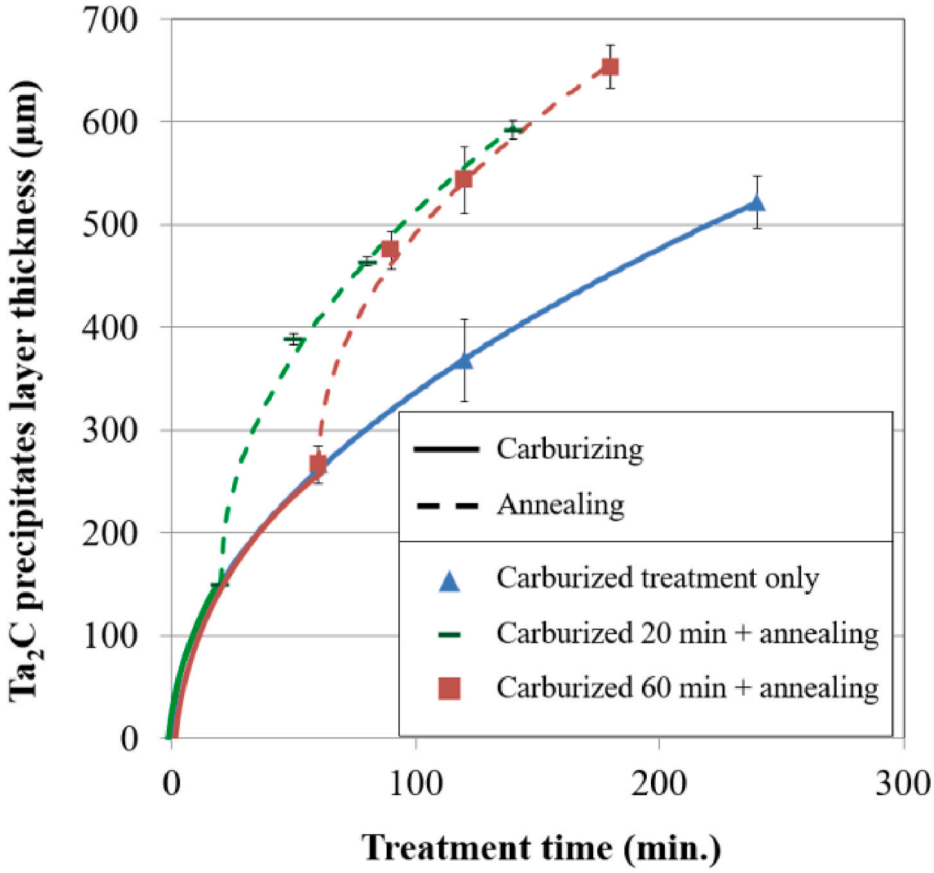


**Fig. 10.** $Ta_2C$ precipitates layer thickness vs. treatment time for carburized and carburized + annealed samples.

confirms that the initial TPL has an influence on the TPL generated after the annealing treatment. Fig. 7 shows obviously that the annealing time has an influence on the higher $Ta_2C$ precipitates depth location (from 400 to 600 µm) and density (from 37 to ~40%) as annealing time varied from 30 to 240 min. The increasing $Ta_2C$ precipitates depth location is due to the diffusion of carbon in the tantalum bulk.

**Table 5**

Growth constants computed from parabolic growth of TPL.

| | Growth constants ($\mu m^2/s$) |
|---|---|
| Only carburized | 18.9 |
| Carburized 20 min + annealing | 27.4 |
| Carburized 60 min + annealing | 21.1 |

*3.2.2. $Ta_2C$ precipitates growth in the TPL*

The nature of the treatment changes the growth of the $Ta_2C$ precipitates in the TPL. Fig. 9 a) shows a TPL produced after a carburizing of 240 min at 1600 °C while Fig. 9 b) shows a TPL produced after a carburizing of 60 min at 1600 °C followed by an annealing of 60 min at 1600 °C. As the thickness of both TPL is similar, it is therefore possible that the annealing treatment increases the TPL growth rate.

In order to understand why an increase of the TPL growth rate occurred during the annealing treatment, the TPL thicknesses were measured on carburized and annealed samples. As mentioned above in paragraph 3.1, the TPL growth kinetic follows a parabolic law as shown in Fig. 10. It is also obvious in Fig. 10 that the annealing treatment accelerate the TPL growth kinetics. The TPL growth kinetics is also described by parabolic laws converging whatever the initial carburizing time.

It is noteworthy in Fig. 9 that the parabolic curve representing the $Ta_2C$ precipitates is reinitialized at the beginning of the annealing treatment causing an increase of the TPL growth kinetics. The corresponding growth constants were measured on the parabolic parts of the different curves of Fig. 9 and reported in Table 5.

An annealing treatment carried out after a carburizing one induced an increase of the TPL growth constants. Besides, the higher the initial carburizing time, the lower is the growth constant.

To explain the above results, we suggest that two phenomena occurred: the first one is the $Ta_2C$ precipitation (during the carburizing cycle) and the second one is the diffusion of carbon into the tantalum matrix. Indeed, the parabolic growth of the TPL is due to the decrease of the carbon flux during a carburizing cycle. According to the first Fick's Law (equation (2)), the carbon flux between two points is driven by three parameters: the carbon diffusion coefficient, the gradient of concentration and the distance between these two points.

$$J = -D\frac{dC}{dx} \tag{2}$$

where $D$ is the diffusion coefficient, $C$ is the concentration of species and $x$ is the distance.

If we have a carbon unsaturated tantalum matrix, the carbon concentration is assumed to be comprised between 0 and its limit of solubility in tantalum at the carburizing temperature [29]. When the carbon diffuses into tantalum, its diffusion coefficient is supposed to be constant. Then, if the sample is carbon unsaturated, the difference between the lowest and the highest carbon concentration is constant. That is why the parabolic growth of TPL can only be explained by the increasing distance between the two extreme carbon concentrations in the tantalum.

At the beginning of the carburizing cycle, the carbon flux is high because of the significant gradient of carbon concentration between the tantalum matrix and carbides layers at the tantalum surface. The increasing carbon concentration in the tantalum induces a decreased carbon flux. The TPL growth is then slow down, as a parabolic law. Therefore, the TPL growth rate involves an increased carbon flux in the tantalum. This growth rate would take place during the annealing treatment. Fig. 11 shows an outline of the carbon concentration evolution, before (Fig. 11 a) and after (Fig. 11 b) the cooling stage of the carburizing cycle. These curves are deducted from the literature [11,13,24].

During the cooling stage, the decrease of the temperature causes the decrease of the limit of solubility of the carbon in the tantalum, which induces $Ta_2C$ precipitation. After cooling, the carbon concentration is equal to its limit of solubility at room temperature, which is very low and estimated to $5.10^{-3}$ % wt [13]. At the beginning of the annealing treatment, the limit of solubility of the carbon in the tantalum increases with the temperature. One can suppose that precipitates do not immediately dissolve with the increasing of carbon solubility limit. Simultaneously, the carbon concentration in the tantalum matrix is still low. Therefore, there is a significant concentration gradient between the tantalum matrix and the carbide layers, increasing the carbon flux in the tantalum matrix. This hypothesis would explain the growth rate increase noticed at the beginning of the annealing treatment. This phenomenon has been also noticed in the literature, with the carburizing of tantalum-tungsten alloy [30].

A convergence of kinetic laws of TPL was noticed in Fig. 10. TPL growth is faster for an initial 20 min carburizing treatment than for a 60 min one. This can be explained by the carbon concentration gradient, higher for 20 min of carburizing than for 60 min.

## 4. Conclusions

In one hand, series of tantalum carburizing has been carried out by low pressure carburizing under ethylene. Optical cross section images have shown that a TPL is obtained, in addition to the TaC and $Ta_2C$ surface layers. This TPL is induced by the precipitation of supersaturated carbon in tantalum during the cooling stage of the carburizing cycle. The TPL thickness measurements have shown a parabolic evolution as a

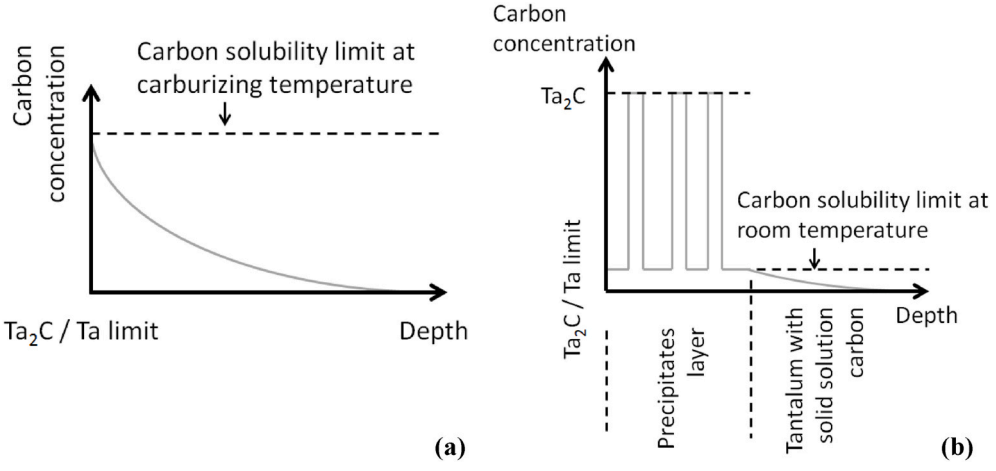


**Fig. 11.** Carbon concentration in tantalum, (a) during a carburizing treatment, (b) after the cooling stage.

function of the carburizing time. This indicates that TPL growth kinetic is driven by carbon diffusion. The $Ta_2C$ precipitation mechanism, described by Dahmen et al. [18], fits well with the observations carried out by optical microscopy. The $Ta_2C$ needs close vacancies to precipitate. Then, if vacancy sinks are at the bulk surface, in a grain boundary or in a dislocation, then the $Ta_2C$ precipitation is highly reduced.

In the other hand, annealing treatments were carried out on carburized samples. The first significant effect of annealing treatments on TPL is the appearance of an almost precipitates free zone near the bulk surface. When the carburized and carburized + annealed samples were compared, it was shown that new $Ta_2C$ precipitates did not form where a previous $Ta_2C$ precipitation occurred. This phenomenon is also explained by Dahmen's mechanism [18]. The vacancies are filled during the first precipitation occurring after the first carburizing cycle. At the end of the annealing treatment, the carbon has diffused deeper in the tantalum. Then, the $Ta_2C$ precipitation is inhibited where the new TPL appeared, and occurred deeper in the tantalum matrix where vacancies are still present. The second significant effect of the annealing treatment is an increase of the TPL growth rate. This was explained by a carbon flux variation, due to the intermediate precipitation of $Ta_2C$ between the carburizing and the annealing treatment. This mechanism needs to be confirmed with additional studies.

**Dominique Cotton:** Investigation, Conceptualization, Methodology, Writing – original draft, Data curation, Formal analysis. **Philippe Jacquet:** Supervision, Writing – review & editing, Resources, Funding acquisition. **Sébastien Faure:** Supervision, Funding acquisition, Writing – review & editing. **Vincent Vignal:** Supervision, Writing – review & editing, Resources, Funding acquisition, Project administration.

The authors declare that they have no known competing financial interests or personal relationships that could have appeared to influence the work reported in this paper.

## Acknowledgements

The authors would like to thank the Burgundy regional council and the CEA for its financial support, and Corinne Nouveau from LaboMaP for helpful comments about this paper.

## References

[1] F.H. Ellinger, The tantalum - carbon system, Transactions of the American Society for Metals 31 (1943) 89–104.
[2] M. Rocher, Carburation d'un métal réfractaire et de ses alliages, Mécanismes et Modélisation, Ecole Nationale Supérieure des Mines de Saint Etienne, France, PhD thesis N°274TD, 2002.
[3] R. Resnick, R. Steinitz, L. Seigle, Determination of diffusivity of carbon in tantalum and columbium carbides by layer-growth measurement, Transactions of the Metallurgical Society of AIME 233 (1965) 1915–1918.
[4] E. Fromm, E. Gebhardt, U. Roy, Diffusion des Kohlenstoffs in den Karbidphasen des Tantals, Z. Metallkd. 57 (1966) 808–811.
[5] N.H. Krikorian, T.C. Wallace, R. Krohn, M.G. Bowman, Formation of Carbide Surfaces on Tantalum and Tantalum-Tungsten Alloys, Los Alamos National Laboratory, 1968. LA-AC-8803.
[6] W.F. Brizes, Diffusion of carbon in the carbides of tantalum, J. Nucl. Mater. 26 (1968) 227–231.
[7] R. Lesser, G. Brauer, Karbidphasen des Tantals, Z. Metallkd. 49 (1958) 622–626.
[8] A.I. Gusev, A.S. Kurlov, V.N. Lipatnikov, Atomic and vacancy ordering in carbide Zeta $Ta_4C_{3-X\ (0.28\ x\ 0.4)}$ and phase equilibria in the Ta-C system, J. Solid State Chem. 180 (2007) 3234–3246.
[9] E.K. Storms, «The Refractory Carbides», Academic Press, New York and London, 1967, pp. 82–93.
[10] A.L. Bowman, The crystal structures of $V_2C$ and $Ta_2C$, Acta Crystallogr. 19 (1965) 6–9.
[11] E. Rudy, D.P. Harmon, Ternary Phase Equilibria in Transition Metal-Boron-Carbon-Silicon Systems vol. V, 1965. Technical report No. AFML-TR-65-2, part I.
[12] R.A. Morris, B. Wang, L.E. Matson, G.B. Thompson, Microstructural formations and phase transformation pathways in hot isostatically pressed tantalum carbides, Acta Mater. 60 (2012) 139–148.
[13] R.W. Powers, M.V. Doyle, Carbon tantalum internal friction peak, J. Appl. Phys. 28 (1957) 255–258.
[14] G. Hörz, K. Lindenmaier, R. Klaiss, High-temperature solid solubility limit of C in Nb and Ta, J. Less Common Met. 35 (1974) 97–105.
[15] D.A. Vaughan, O.M. Stewart, C.M. Schwartz, «Determination of Intertitial Solid Solubility Limit in Tantalum and Identification of the Precipitate Phase», Battelle Memorial Institute, 1960. Technical Report No. BMI-1472.
[16] M.L. Pochon, C.R. McKinsey, R.A. Perkins, W.D. Forgeng, «Solubility of carbon and structure of carbide phases in tantalum and columbium», reactive metals, Proceedings of Metallurgical Society Conference (1959) 327–347.
[17] U. Dahmen, Microstructures and Phase Transformations in Interstitial Alloys of Tantalum, PhD thesis, Lawrence Berkeley National Laboratory, 1979. LBNL Paper LBL-8661.
[18] U. Dahmen, K.H. Westmacott et, G. Thomas, A study of precipitation in interstitial alloys -I. Precipitation sequence in Ta-C alloys, Acta Metall. 29 (1980) 627–635.
[19] K.M. Axler, Processing and characterization of engineered materials in the tantalum carbon system, in: First International Conference on Processing Materials for Properties, 1993.
[20] P.J. Rodriguez, Characterization and Refinement of Carbide Coating Formation Rates and Dissolution Kinetics in the Ta-C System, Los Alamos National Laboratory, LA-13173-T, 1996.
[21] J.A.H. De Pruneda, Reusable Crucible for Containing Corrosive Liquids, vol. 383, Lawrence Livermore National Laboratory, 1995, p. 981. Patent No. 5.
[22] P.C. Lopez, P.J. Rodriguez, R.A. Pereyra, Packed Bed Carburization of Tantalum and Tantalum Alloy, vol. 916, Los Alamos National Laboratory, 1998, p. 377. Patent No 5.
[23] B.H. Eckstein, R.F. Forman, Preparation and some properties of tantalum carbide, J. Appl. Phys. 33 (1962) 82–87.
[24] E. Fromm, U. Roy, The high-temperature solid solubility limit of carbon in tantalum, J. Less Common Met. 8 (1965) 73–75.
[25] W.H. Chang, J.W. Clark, G.D. Oxx Jr., Tantalum-base Alloys, vol. 379, 1968, p. 520. Patent n°3.
[26] G.V. Kidson, Some aspects of the growth of diffusion layers in binary systems, J. Nucl. Mater. 1 (1961) 21–29.
[27] L.B. Vasilenok, E.N. Kablov, B.S. Bokshtein, I.M. Razumovskii, Diffusion of carbon along grain boundaries in niobium, Dokl. Phys. 45 (2000) 588–591.
[28] K.H. Westmacott, M.I. Perez, The co-precipitation of vacancies and carbon atoms in quenched platinum, J. Nucl. Mater. 83 (1979) 231–237.
[29] J.S. Kirkaldy, Diffusion in multicomponent metallic systems: III. The motion of planar interfaces, Can. J. Phys. 36 (1958) 917–925.
[30] L. Carette, "Etude des mécanismes de formation des carbures obtenus par cémentation basse pression d'un alliage de tantale, application à la pyrochimie", Ecole Nationale Supérieure d'Arts et Métiers, France, PhD Thesis N°2019-ENAM-0029, 2019.